Lateral migration of peptides in transversely sheared flows in water: an atomistic-scale-resolving simulation

Fan Li[1], Ivan Korotkin[2], Vladimir Farafonov[3], and Sergey A. Karabasov[1]

[1] The School of Engineering and Materials Science, Queen Mary University of London, Mile End Road, E1 4NS London, United Kingdom

[2] Mathematical Sciences, University of Southampton, University Road, SO17 1BJ Southampton, United Kingdom

[3]Department of Physical Chemistry, V. N. Karazin Kharkiv National University, Svobody Sq. 4, Kharkiv, 61022, Ukraine

Email: s.karabasov@qmul.ac.uk

Abstract

For atomistic scale-resolving simulations of peptide diffusion, which are representative of molecular sorting in micro-fluidic device, a hybrid Fluctuating Hydrodynamics - Molecular Dynamics (FH/MD) model is implemented based on the two-phase flow analogy framework. Thanks to the used framework, in comparison with existing simulations in the literature, the suggested model captures inter-atomic forces between the peptides and the surrounding shell of water atoms at atomistic resolution while concurrently taking into account the non-uniform flow effect. In comparison with previous applications of the hybrid two-phase flow analogy method, multiple moving atomic-resolution zones are implemented for the first time here. The moving zones comprise one and two peptides solvated in water with a Poiseuille flow applied, where each diffusing peptide and the surrounding water shell are dynamically resolved. The models are validated in comparison with the pure all-atom molecular dynamics simulations for the no flow case and then used to investigate how the flow rate and the starting location of peptides in the parabolic flow profile affect their lateral migration over a range of flow Reynolds numbers. It is estimated that for the Poiseuille flows considered, the FH/MD model is 2 to 20 times faster in

comparison with the conventional all-atom non-equilibrium molecular dynamics simulations.

1. Introduction

In the nearest future, micro- and nano-fluidic devices are likely to revolutionise techniques used for multiphase flow analysis, sensor design, and molecular and cellular sorting. In comparison with traditional bench-scale systems, microfluidic devices are especially advantageous because of their low fabrication costs, less material and reagent consumption, improved performance, reduced measurement time, and higher processing speed [1, 2]. In biomedical sciences, microfluidic sorting techniques allow one to separate small concentrations of particles in multi-phase solutions in accordance with mechanical properties such as the particle size, shape and deformability. For example, [3] showed how a peptide solution can be cleaned from initially present bacteria and blood cells by filtering it out through a microchannel of a micro-fluidic device at a controlled flow rate. As another example, [4] shows how a micro-fluidic device can efficiently replace the labour-intensive manual cell staining and washing. The applied technology is based on the particle sorting that enables the cell to migrate from the suspension to the reagent stream once the two flows are put in contact in a specially designed microchannel. Importantly, one feature in common for many micro-fluidic technologies is a precise control of the particle diffusion by inducing a shear flow gradient leading to lateral migration of the cells and molecules being sorted.

Flow-induced particle diffusion in conventional suspensions, such as where the particle diameter reaches a sub-millimeter size while the width of the flow channel is in the order of a few millimeters, has been widely investigated using continuum mechanics approaches since 1960s [5]. The existing mathematical models of diffusion in conventional suspensions can be cast into two categories: diffusive flux and suspension balance methods. Both of them are based on approximations of continuum hydrodynamics effects. In diffusive flux methods, the particle diffusion is modelled as a process dependent on some effective bulk flow velocity, viscosity and concentration gradient [6]. In suspension balance methods, the stress exerted from the flow on a particle is expressed via an empirical constitutive relation and the transport equations are solved by rheological models [7]. Significant efforts were devoted to refining and improving the semi-empirical particle diffusion models in order to quantitatively predict the particle migration process and concentration [8-13].

In comparison with conventional suspensions, the particles used in many micro- and nano-fluidic applications, such as molecules, are smaller than 100 nm where the Brownian motion is essential. To model such systems, mesoscopic methods have been proposed in the literature such as the Eulerian-Lagrangian model [14, 15], where particles are treated as a discrete Lagrangian phase suspended in a continuum Eulerian fluid. The particles' motion satisfies Newton's second law, while the coupling between the fluid and the particles is modelled by including the sources term in the fluid equations. The latter include both the deterministic and the random Brownian force. Models of this type allow capturing some of the molecular diffusion effects. For example, the enhanced heat transfer of Alumina-water solution in comparison with the pure water was simulated in [16], which was attributed to the lateral migration of the Alumina particles. The model included both the Brownian and the temperature gradient-based (thermophoretic) force effects. Despite the success of mesoscopic methods, the force fields they use (such as the ones based on statistical modelling approaches) are applicable for relatively large particles, and their application to nanoscale particle problems is debatable. For example, van der Waals and electrostatic forces emerging at the micro- and nanoscale are not resolved in the mesoscopic models despite their importance for particle transport in micro-fluidic devices [17, 18].

Although the van der Waals and electrostatic forces had been taken into account in the lattice Boltzmann method for polymer chain simulations [19, 20], this coarse-grain modelling missed atomistic details at the interatomic level. Molecular Dynamics (MD) simulations provide the description of molecular diffusion processes at the microscale resolution level. However, this resolution comes at a high computational cost especially when macroscopic flow effects need to be taken into account. So far only few studies have focused on the modeling of particle diffusion in MD simulations. For instance, MD was used in [21] to investigate the dispersion of copper (Cu) nanoparticles in liquid argon in a nano-channel under rather high flow velocity strain rates, the particle transport was directly simulated in both the stream-wise and transverse flow directions. The particle motion in the transverse directions appeared to be completely Brownian while no lateral migration was reported in the shear direction. Notably, simulations of the flow effect on molecular diffusion are typically performed with Non-Equilibrium MD (NEMD) methods, which require several orders of magnitude higher flow rates in comparison with the experimental conditions in order to accelerate the statistical convergence of the MD solution [21, 22]. This explains the

difficulty of mimicking relevant molecular diffusion regime typical of micro-fluidic devices. To the best knowledge of the authors, no pure all-atom MD method has been applied to simulate the lateral migration of nano-size particles.

On the other hand, the migration of nano-scale particles in micro-fluidic devices can be modelled by hybrid multiscale methods, which retain the all-atom resolution in a small vicinity of the particle, while representing the rest of the fluid by much more computationally efficient macroscopic models based on continuum mechanics. For example, Domain Decomposition and Heterogeneous Multiscale Methods (DDM and HMM) [23-25] can be used to establish the 'hand shaking' between the MD particles and the continuum fluid dynamics (CFD) representation of the same liquid.

HMM typically embeds a micro model described by an interaction potential between discrete particles in the nodes of a uniform Cartesian grid that covers the entire macroscopic simulation domain where Navier-Stokes (NS) equations are solved. Within this approach, a macroscopic solution is used to enforce a prescribed strain rate or a mass flux at the boundaries of the microscopic model. The same stresses are then obtained by averaging the microscopic solution in order to feed them back to the momentum component of the Navier-Stokes equations at the next iteration step [23, 25]. A further advancement of HMM, the so-called internal-flow multiscale method (IMM) was developed, where the microscopic model does not necessary collocate with a grid node of the continuum solver. Both methods have been successfully applied to simulate flow in carbon nanotubes, flow in axially-periodic converging/diverging nano-channels, and flow through membranes [23, 25, 26]. However, so far neither of these methods have been extended to the modelling of molecular diffusion of nano-size particles. This can be attributed to the fact that the location of the microscopic part of both the HMM and IMM models is fixed with respect to the Eulerian grid thereby making it difficult to capture the three-dimensional trajectory of atomistic particles of interest concurrently with the update of the macroscopic part of the solution.

On the DDM front, the coupling of MD equations with Computational Fluid Dynamics was pioneered by O'Connell and Thompson for the Lennard-Jones fluid [27]. In the original work, the CFD model utilised the solution of steady Navier-Stokes equations, whereas further investigations used a more advanced Landau and Lifshitz Fluctuating Hydrodynamics (LL-FH) model [28], which not only satisfies the macroscopic fluid dynamics solution but also preserves statistical variances of

thermal density and velocity fluctuations due to the Brownian motion [29-31]. Depending on how the information is transferred between the MD and CFD regions, the domain decomposition method can be classed into flux coupling and state coupling schemes. In the flux coupling scheme, the momentum and mass fluxes of the non-overlapping MD and CFD regions are exchanged via a boundary condition at the interface to preserve the corresponding conservation laws. It is straightforward to reconstruct the flux from MD zone to CFD zone by averaging the microscopic solution, however, the opposite in non-trivial [32, 33]. Alternatively, in the state coupling schemes, a finite overlap region is used between the MD and CFD zones. In the overlap region, macroscopic fluxes of mass and momentum are reconstructed and the particle equations of motion are modified to include the macroscopic forcing effect [27, 34]. The finite overlap region allows for a smoother transition between the particle dynamics and continuum in comparison with the flux coupling method using some interpolation parameter[27, 34]. The accuracy maybe further improved by incorporation of multi-resolution particle models [35, 36]. Nevertheless, due to the complexity of multi-resolution methods of this sort they have not been extended to particle diffusion modelling yet.

The current work follows the hybrid modelling approach developed in [37-40]. This model is of state-variable coupling type where the macroscopic and the microscopic parts are regarded as two nominal “phases” of the chemical substance, which are coupled by the conservation laws of mass and momenta. One phase stands for a continuum mechanics representation and the other phase stands for a discrete atomistic phase representation; the concentration of the atomistic phase is a user-defined function that determines the multiscale model resolution. The continuum phase is governed by the equations of Landau and Lifshitz Fluctuating Hydrodynamics-type. In order to avoid artificial phase separation, forcing terms are introduced in the MD particle equations, which are accounted for in the macroscopic flow equations to preserve the conservation laws of mass and momentum of the two-phase mixture. In [41-43] it was shown that, when implemented in GROMACS [44], a simplified one-way coupled version of the original method, which accounts for the flow effect on microscopic particles, is sufficiently accurate for simulations of a wide range of problems such as molecular diffusion [41, 42, 45], oscillations of a PCV2 virus capsid in water in equilibrium conditions [42, 43], and the interaction of nano-confined water with material surfaces of an Atomic Force Microscope [46].

In the current work, this hybrid multiscale method is applied to simulate diffusion of peptides in water under Poiseuille flow conditions. The goal of the simulations is to investigate the effect of parameters, which could be controlled in a micro-fluidic experiment, such as the flow Reynolds number and the initial location where peptides are introduced in the flow, on the lateral migration process.

The paper is organised as follows. The hybrid multiscale method based on the two-phase analogy model is summarised in Section 2.1 and its suggested modification to simulate multiple MD zones locked to the centres of mass of moving molecules of interest in a Poiseuille flow is presented in Section 2.2. Numerical simulation results are presented and discussed in Section 3.

2. Computational methodology

2.1 The two-phase flow analogy method for concurrent multi-resolution simulations from continuum to atomistic scales

In the framework of the hybrid continuum-atomistic model [40-42], the large-scale continuum and the small-scale discrete particles representation of same liquid are considered as "phases" of a nominally two-phase liquid. The phases satisfy conservation laws of mass and momentum and their concentrations are $0 \le s \le 1$ and $0 \le 1-s \le 1$ for the continuum phase and for the atomistic phase, respectively. The concentration is a user-defined function that determines the model resolution – from atomistic (s=0) to continuum (s=1). This function naturally comes in the conservation laws for mass and momentum of the continuum phase:

$$\delta_t(sm) + \sum_{\gamma=1,6} (s\rho\tilde{\boldsymbol{u}})\, d\boldsymbol{n}^r \delta t = \delta_t J^{\rho}, \tag{1}$$

$$\delta_t(smu_i) + \sum_{\gamma=1,6} (s\rho u_i\tilde{\mathbf{u}}) d\mathbf{n}^r \delta t = s \sum_{j=1,3} \sum_{\gamma=1,6} \left(\Pi_{ij} + \Pi'_{ij}\right) d\mathrm{n}_j^{\gamma} \delta t + \delta_t J_i^{\mathbf{u}}, i = 1,2,3 \tag{2}$$

and the same of the atomistic particle phase

$$\delta_t\left((1-s)\sum_{p=1,N_{(t)}} m_p\right) + \sum_{\gamma=1,6}\left((1-s)\sum_{p=1,N_{\gamma(t)}} \rho_p\, \mathbf{u_p}\right) d\mathbf{n}^r \delta t = -\delta_t J^{\rho} \tag{3}$$

$$\delta_t\left((1-\mathrm{s})\sum_{p=1,N(t)} m_p u_{ip}\right)+\sum_{\lambda=1,6}\left((1-s)\sum_{p=1,N_{\gamma(t)}}\rho_p u_{ip}\,\mathbf{u_p}\right)d\mathbf{n}^r\delta t = \\ =(1-s)\sum_{p=1,N(t)} F_{ip}\delta t-\delta_t J_i^{\mathbf{u}} \qquad ,i=1,2,3 \tag{4}$$

of the two-phase fluid.

In the above equations, the fields with a sub-index p corresponds to the particles while the cell-volume and cell-flux averaged values do not contain the particle sub-index. $\rho_p=\frac{m_p}{V}$ is the density of the atomistic phase, which occupies the elementary cell V. m_p ,$\mathbf{u}_p$ are the particle mass and velocity. ρ is the density of the continuum phase and $\tilde{\mathbf{u}}$ stands for the velocity vector of the two-phase mixture $\tilde{u}_i=\left[s\rho u_i+(1-s)\sum_{p=1,N(t)}\rho_p u_{ip}\right]/\tilde{\rho}$, where u_i is velocity of continuum hydrodynamic phase, which corresponds to the deterministic and stochastic parts of the Reynolds stress, Π and Π', respectively. N_t is the number of particles in elementary cell V. $N_\gamma(t)$ is the number of particles crossing the normal $d\mathbf{n}^r$ of γ surface and $\bar{\rho}$ is the mixture density, $\tilde{\rho}=s\rho+(1-s)\sum_{p=1,N(t)}\rho_p$. δ_t denotes the change of mass and momenta over time δt, which in case of the atomistic particles plays the role of the particle counter for mass and momenta in control volume V over time δ_t.

The source terms $\delta_t J^\rho$ and $\delta_t J_i^{\mathbf{u}}$ are input functions of the hybrid model. They depend on the user-defined phase concentration function s and are needed to suppress the artificial phase separation. These functions are selected in such a way to drive the differences from the target cell-averaged particle values and the two-phase mixture cell-averaged density and momenta , $\tilde{\rho}-\sum_{p=1,N_\gamma(t)}\rho_p$ and $\tilde{\rho}\cdot\tilde{u}_i-\sum_{p=1,N(t)}\rho_p u_{ip}$, to zero

The system of mass and momentum equations (3),(4) can be rearranged and solved numerically together with the Molecular Dynamics [38, 39]. These equations converge to the standard Landau-Lifshitz Navier-Stokes Fluctuating Hydrodynamics equations in the limit of s=1 when the source terms dependent on the particle fields in Eqs (1) and (2) vanish to zero.

The two-phase analogy model is closed by including appropriate continuum-discrete forcing terms in the Molecular Dynamics (MD) equations $\frac{d\mathbf{x}_\mathrm{p}}{dt}=\mathbf{u}_\mathrm{p}$, $\frac{d\mathbf{u}_\mathrm{p}}{dt}=\mathbf{F}_\mathrm{p}/m_p$ ($\mathbf{x}_\mathrm{p}$, $\mathbf{u}_\mathrm{p}$, $\mathbf{F}_\mathrm{p}$ and m_p are particle coordinate, velocity, interatomic potential force and particle mass) to obtain:

$$\frac{d\mathbf{x}_\mathrm{p}}{dt} = \mathbf{u}_\mathrm{p} + s\left(\tilde{\boldsymbol{u}} - \mathbf{u}_\mathrm{p}\right) + \alpha(1-s)\mathrm{s}\cdot\frac{\sum_{\gamma=1,6}\left(\tilde{\rho} - \sum_{p=1,N_\gamma(t)}\rho_p\right)d\mathbf{n}^r}{\sum_{p=1,N(t)}m_p} \tag{4}$$

$$\frac{du_{ip}}{dt} = (1-s)F_{ip}/m_{ip} + \\ + \frac{\sum_{k=1,3}\sum_{\gamma=1,6}\left(\alpha(1-s)\mathrm{s}\cdot\sum_{p=1,N(t)}\rho_p\cdot u_{ip}\left(\frac{\sum_{\lambda=1,6}\left(\tilde{\rho}-\sum_{p=1,N(t)}\rho_p\right)dn_k^\lambda}{\sum_{p=1,N(t)}m_p}\right)\right)dn_k^\lambda}{\sum_{p=1,N(t)}m_p} \\ + \frac{\sum_{k=1,3}\sum_{\gamma=1,6}\left(\beta(1-s)\mathrm{s}\cdot\frac{1}{V}\left(\sum_{\lambda=1,6}\left(\tilde{\rho}\cdot\tilde{u}_i-\sum_{p=1,N(t)}\rho_p u_{ip}\right)dn_k^\lambda\right)\right)dn_k^\gamma}{\sum_{p=1,N(t)}m_p},\ \ i=1,2,3, \tag{6}$$

where $\tilde{\boldsymbol{u}}$ and $\tilde{\rho}$ are the velocity vector and density of the two-phase mixture, $\sum_{p=1,N(t)}\rho_p$ and $\sum_{p=1,N(t)}\rho_p u_{ip}$ are cell-averaged fields of the MD particle densities and velocity in the elementary Eulerian cell where the particle of interest resides at the moment. To preserve continuity, the field values corresponding to the particle coordinates are obtained by interpolation using the fields from adjacent elementary volumes. $\alpha \geq 0$ and $\beta \geq 0$ are adjustable functions which control how fast the parameters of the particle phase equilibrate to the continuum flow values.

The forcing terms on the right-hand-side are defined consistently with the $\delta_t J^\rho$ and $\delta_t J_i^{\mathbf{u}}$ fields to preserve the conservation of mass and momentum. In the limiting states $s = 0$ and $s = 1$, the corresponding source terms are zero because of the $(1-s)\mathrm{s}$ multiplier. Notably, at $s = 0$ the above particle equation reduce to the pure molecular dynamics.

2.2 The one-way coupled hybrid multiscale model for bimolecular diffusion in Poiseuille flow

Diffusion of small biomolecules is considered in a planar Poiseuille flow typical of nano-fluidic devices. The solution of the Poiseuille flow is given by [47]

$$\left.\begin{array}{c}\left(\rho_0, \boldsymbol{u}^{Poiseuille}\right) = (\rho_0, u_1, u_2, u_3) \\ u_1 = \frac{dp/dx_1}{2\mu}\left(L^2/4 - {x_3}^2\right) \\ u_2 = 0 \\ u_3 = 0\end{array}\right\} \tag{5}$$

where μ is dynamic viscosity and $L/2$ is a half-height of the cubic computational domain. The pressure gradient, dp/dx_1 is set to drive the flow with prescribed flow rates, $u_{max} = L^2\frac{dp/dx_1}{8\mu} =$ 0.03, 0.04, 0.055, 0.07, 0.075 and 0.1 nm/ps corresponding to a range of Reynolds numbers, $Re = \frac{u_{max}L}{\nu} = 0.25 - 0.8$ typical of microfluidic devices based on the kinematic viscosity of water ν=1.004 10^{-6} m^2/s. Notably, $u_{max} = 0.03$ nm/ps is a few orders of magnitudes

smaller in comparison with flow velocity values typically used in Non-Equilibrium MD (NEMD) methods, where the flow velocity would be required to be in the order of the thermal molecular speed in order to reduce the numerical noise due to insufficient statistical averaging.

To include the thermal density and velocity fluctuations, which are important for nano-scale particle diffusion, thermal density and velocity fluctuations $\left(\rho'(\boldsymbol{x},\mathrm{t}),\mathbf{u}'(\boldsymbol{x},\mathrm{t})\right)$ are included,

$$(\rho,\mathbf{u})^{total}(\boldsymbol{x},t)=\left(\rho_0+\rho'(\boldsymbol{x},t),\boldsymbol{u}^{Poiseuille}(\boldsymbol{x})+\boldsymbol{u}'(\boldsymbol{x},t)\right), \tag{6}$$

where the fluctuation part, $\left(\rho(\boldsymbol{x},\mathrm{t}),\mathbf{u}'(\boldsymbol{x},\mathrm{t})\right)$ satisfies the free-space LL-FH equations

$$\frac{\partial\rho}{\partial t}+\mathrm{div}(\rho\cdot\mathbf{u}')=0 \tag{9}$$

$$\frac{\partial(\rho\cdot u_i')}{\partial t}+\mathrm{div}(\rho\cdot u_i'\cdot\mathbf{u}')=\sum_{i,j=1,3}\nabla_j\left(\Pi_{ij}+\Pi'_{ij}\right), \tag{10}$$

and where the deterministic and stochastic fluctuating Reynolds stresses Π_{ij} and Π'_{ij} are given by

$$\Pi_{ij}=-p'(\rho)\delta_{ij} \tag{11}$$

$$\Pi'_{ij}=\xi\mathrm{div}\,\mathbf{u}'\delta_{ij}+\eta\left(\partial_i u_j'+\partial_j u_i'-2D^{-1}\mathrm{div}\mathbf{u}'\delta_{ij}\right) \tag{12}$$

where $i,j=1,2,3$, ξ and η are shear and bulk water kinematic viscosity coefficients, p' is the pressure fluctuations induced by the density fluctuation. According to the fluctuation-dissipation theorem, the covariance of the stochastic stress tensor Π'_{ij} is expressed as follows

$$\langle\Pi'_{ij}(r_1,t_1)\Pi'_{kl}(r_2,t_2)\rangle=2k_bT\left[\eta\left(\delta_{ik}\delta_{jl}+\delta_{il}\delta_{jk}\right)+(\xi-2D^{-1}\eta)\delta_{ij}\delta_{kl}\right]\times\delta(t_1-t_2)\delta(r_1-r_2) \tag{7}$$

Following the statistic mechanics theory [28], stochastic stress tensor can be expressed as follows

$$\Pi'_{ij}=\sqrt{\frac{2k_bT}{\delta t\delta V}}\left(\sqrt{2}\sqrt{\eta}\cdot\mathbf{G}^{\mathbf{S}}_{\mathbf{ij}}+\sqrt{D}\sqrt{\xi}\cdot\mathbf{tr}[\mathbf{G}]\cdot\frac{\mathbf{E_{ij}}}{\mathbf{D}}\right) \tag{14}$$

Here $\mathbf{G}$ is random Gaussian matrix whose mean is zero, $\mathbf{G}^{\mathbf{S}}_{\mathbf{ij}}=\frac{G_{ij}+G_{ij}^T}{2}-\mathbf{tr}[\mathbf{G}]\cdot\frac{\mathbf{E_{ij}}}{\mathbf{D}}$, $\mathbf{E}$ is the unite matrix and $\mathbf{tr}[\mathbf{G}]=G_{11}+G_{22}+G_{33}$, which stands for trace of matrix, T,k_b are temperature and Boltzmann constant respectively.

By combining the analytical Poiseuille solution and the numerical LL-FH solution the total continuum hydrodynamic field, $(\rho,\mathbf{u})^{total}$, is obtained. The latter solution includes both the nonuniform macroscopic flow effect and the thermal fluctuation effect and serves as a good approximation of the solution of the two-phase flow analogy equations (1)-(4), $(\tilde{\rho},\tilde{\mathbf{u}})\equiv(\rho,\mathbf{u})^{total}$.

The model (7)-(14) corresponds to a one-way coupled version of two-phase analogy method where the discrete particle phase is decoupled from continuum phase and the MD particles are immersed in the hydrodynamics "bath", which effect becomes dominant for $s \to 1$ [41-43, 45]. In comparison with the fully coupled model, the continuum flow of the one-way coupled model is assumed to satisfy the stochastic Navier-Stokes equations, where the microscopic effects are implicitly included. Hence, all macroscopic parameters of these equations, such as the viscosity coefficient in the stress/strain relationship, need to be appropriately calibrated before using them as the effective external force fields in the modified MD equations (5) and (6) for consistency.

To close the model, the application-specific window function $s(x, y, z, t)$, which controls the hybrid model resolution in locations of interest, needs to be defined. In the current case, the all-atom resolution is essential for each biomolecule and the surrounding water shell while the fully atomistic resolution can be gradually replaced by continuum reduce away from these sensitive regions. Since the number of diffusing biomolecules will vary in current study, another argument n=1,2 is introduced to distinguish between different cases:

$$S(x, y, z, t, 1) = \begin{cases} 0 & r_1(t) \le R_{MD} \\ S_1(t) & R_{MD} < r_1(t) < R_{FH}, \\ S_{max} & r_1(t) \ge R_{FH} \end{cases} \tag{15a}$$

$$S(x, y, z, t, 2) = \begin{cases} 0 & (r_1(t) \le R_{MD}) \cap (r_2(t) \ge R_{FH}) \\ 0 & (r_1(t) \ge R_{FH}) \cap (r_2(t) \le R_{MD}) \\ 0 & (r_1(t) \le R_{MD}) \cap (R_{MD} < r_2(t) < R_{FH}) \\ 0 & (R_{MD} < r_1(t) < R_{FH}) \cap (r_2(t) \le R_{MD}) \\ 0 & (r_1(t) \le R_{MD}) \cap (r_2(t) \le R_{MD}) \\ S_1(t) & (R_{MD} < r_1(t) < R_{FH}) \cap (r_2(t) \ge R_{FH}) \\ S_2(t) & (r_1(t) \ge R_{FH}) \cap (R_{MD} < r_2(t) < R_{FH}) \\ (S_1(t) \times S_2(t))/S_{max} & (R_{MD} < r_1(t) < R_{FH}) \cap (R_{MD} < r_2(t) < R_{FH}) \\ S_{max} & (r_1(t) \ge R_{FH}) \cap (r_2(t) \ge R_{FH}) \end{cases} \tag{15b}$$

In the above expressions $S_i(t)$ $(i = 1,2)$ is given by

$$S_i(t) = \frac{r_i(t) - R_{MD}}{R_{FH} - R_{MD}} S_{max}, \tag{16}$$

where $r_i(t) = (x - c_{ix})^2 + (y - c_{iy})^2 + (z - c_{iz})^2$ stands for the distance from the center of mass of each biomolecule, whose coordinates are $(c_{ix}, c_{iy}, c_{iz})(t)$, and the maximum value is set to $S_{max} = 0.98$. For the one peptide case, Fig.1a shows the layout of the hybrid model where the computational domain decomposition is based on the S-function (15a) corresponding to the initial time moment, $S(x, y, z, 0,1)$. The resolution gradually changes from all-atom (red region),

$S(x,y,z,0,1) = 0$ to atomistic-continuum (white region), $0 < S(x,y,z,0,1) < S_{max}$ and finally to the continuum resolution (white region), $S(x,y,z,0,1) = S_{max}$~1. Notably, in comparison with one peptide, for the two- peptide system, the all-atom resolution zone of the widow function, $S(x,y,z,t,2) = 0$ can be a simply or a multiply connected region, depending on the distance between the two nanoparticles. Schematics of the model configuration for one- and two- peptide case are compared in Fig.1b.

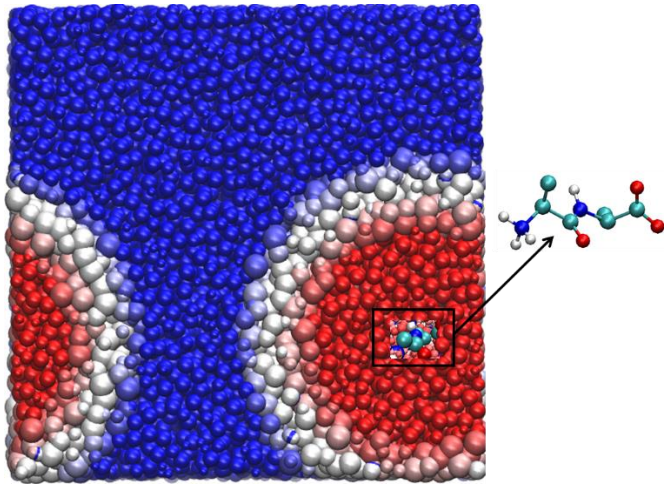

(a)

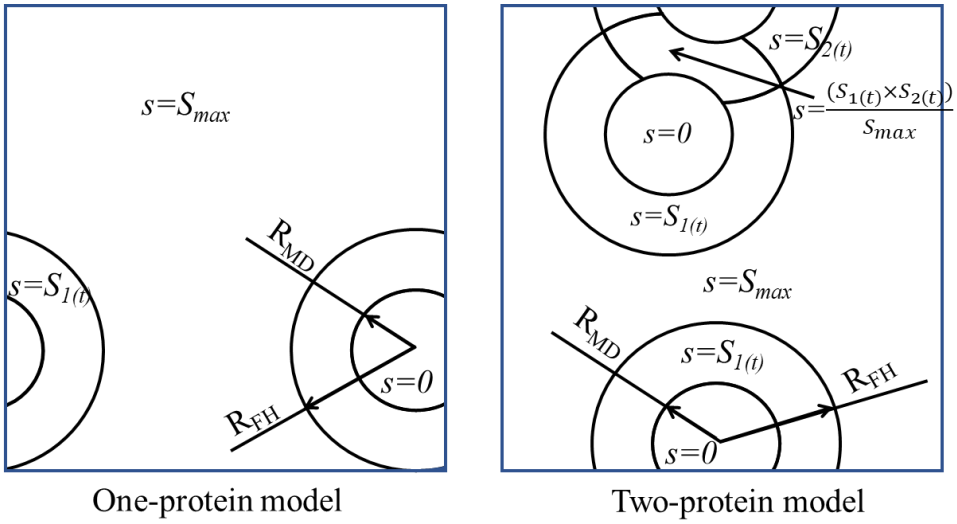

(b)

Fig.1 The simulation domain of the hybrid multiscale method: (a) model details for the one biomolecule case where the peptide is immersed in water and its center is locked to the origin of the window function, $S(x,y,z,0,1)$ and (b) schematics of the one- and two- peptide models.

The entire model, which includes on the LL-FH equations (9)-(14) and modified MD

equations (5),(6),(15a),(15b),(16), is implemented in GROningen MAchine for Chemical Simulations (GROMACS) [44]. The MD simulations are performed at 298 K with Berendsen thermostat in a cubic computational box, (L x L x L)=(8 x 8 x 8) nm^3, which corresponds to (10 x 10 x 10) computational cells of the continuum LL-FH model solved by a finite-volume method [48]. The atomistic water modelling is based on the Extended Simple Point Charge (SPC/E) model and the target water density is set to 1000 kg/m^3. Each simulation run corresponds to 1 ns, the MD time step is 1 fs, and the continuum hydrodynamics time step is set to 10 fs. To improve statistical averaging when computing the diffusion coefficient either with the pure MD or the hybrid FH-MD method, 15 independent runs are performed for each case. In the statistical case, the ensemble averaged diffusion coefficient over 15 runs is equivalent to computing the same coefficient over 15 ns of simulation time since effective correlations in the MD signal decay much faster than one nanosecond. The continuum LL-FH computation corresponds to a small fraction of the cost of the MD model. Electrostatic interactions in the MD model are calculated by the reaction field method with dielectric constant equal to 78. The cut-off distance for electrostatic interaction and van der Waals force is set to 1 nm. A small peptide corresponding to the zwitterionic form of dialanine, is considered. The dialanine molecule compromises two residues and is a popular system in bio-molecular research. The peptide is simulated with the GROMOS 54A7 Force Field [49]. Van der Waals interactions between the water and the peptide are determined by mixing rules. Before performing production runs of the hybrid multiscale model, the MD part of the model is equilibrated by performing all-atom molecular dynamics simulation with no flow for 1 ns. NVT ensemble and triple periodic boundary conditions are used in all MD simulations.

3.Results

3.1 Diffusion of one and two peptides in water without flow

As pointed out by [41], accuracy of the one-way coupled hybrid model is sensitive to the numerical parameters such as the size of the MD/FH buffer zone and the MD zone, R_{MD} and R_{FH} parameters, respectively. In addition, the amplitudes of the forcing terms α and β, which determine the strength of the coupling between the MD equations and the hydrodynamics field should be appropriately calibrated. Following [45], the model calibration step is performed by considering the peptide diffusion in water without any flow and comparing the hybrid method

results with the trajectory solutions obtained from the pure all-atom MD simulations.

For one peptide-system (15a), the peptide molecule (P1) is initialised near the domain centre, $\frac{2x_3}{L} = -0.175$, and the model parameters are $R_{MD} = 0.5L/2$, $R_{FH} = 0.8L/2$, and $\alpha = \beta = 40$ nm^2/ps, which are similar to the ones recommended in [45]. Fig.2a and b shows the resulting time dependency of the ensemble averaged mean square displacement (MSD) of one peptide diffusing in water. It should be noted that while the MSD trajectories have been computed for one nanosecond intervals in all simulations of this article, only the first 800 ps of those are used for the calculation of the diffusion coefficient to eliminate the spurious noise effect due to the open-ended signal.

As expected for the isotropic diffusion case, the MSD trajectories along *x*,*y* and *z* direction are close one to another (in Fig.2a). This suggests that the hybrid model implementation is free from numerical artefacts. The peptide trajectory of the hybrid FH/MD model is in a good agreement with the reference solution of the all-atom MD simulation as shown in Fig.2b. Furthermore, the molecular diffusion coefficient of peptide in water is computed from the slope of the MSD trajectory in accordance with the Einstein relation [50]. The resulting diffusion coefficients obtained by the fits to trajectories shown in Fig.2b are 0.87×10^{-5} cm^2/s and 0.77×10^{-5} cm^2/s for the all-atom MD model and the hybrid FH/MD model, respectively.

To probe sensitivity of the hybrid multiscale model to the α and β coupling parameters, the same single peptide in water at equilibrium conditions is simulated for $\alpha = \beta = 60$ nm^2/ps (50% increase in comparison with the recommended values). The results are shown in Fig.2 (c) and (d). Notably, the MSD trajectories along *x*,*y* and *z* direction are still close one to another as expected for the isotropic diffusion process (Fig.2c). However, the computed diffusion coefficient in this case is 0.54×10^{-5} cm^2/s (Fig.2d), which is 40% smaller than the MD reference and 30% smaller than the model result for $\alpha = \beta = 40$ nm^2/ps case. This indicates that the hybrid model is moderately sensitive to the coupling parameter. This parameter is a calibration coefficient, which needs to be re-evaluated for each system. Hence, given the accurate results produced by the hybrid model at $\alpha = \beta = 40$ nm^2/ps, the latter value of the coupling parameter is used for the simulation of the single peptide in water system where the flow is activated.

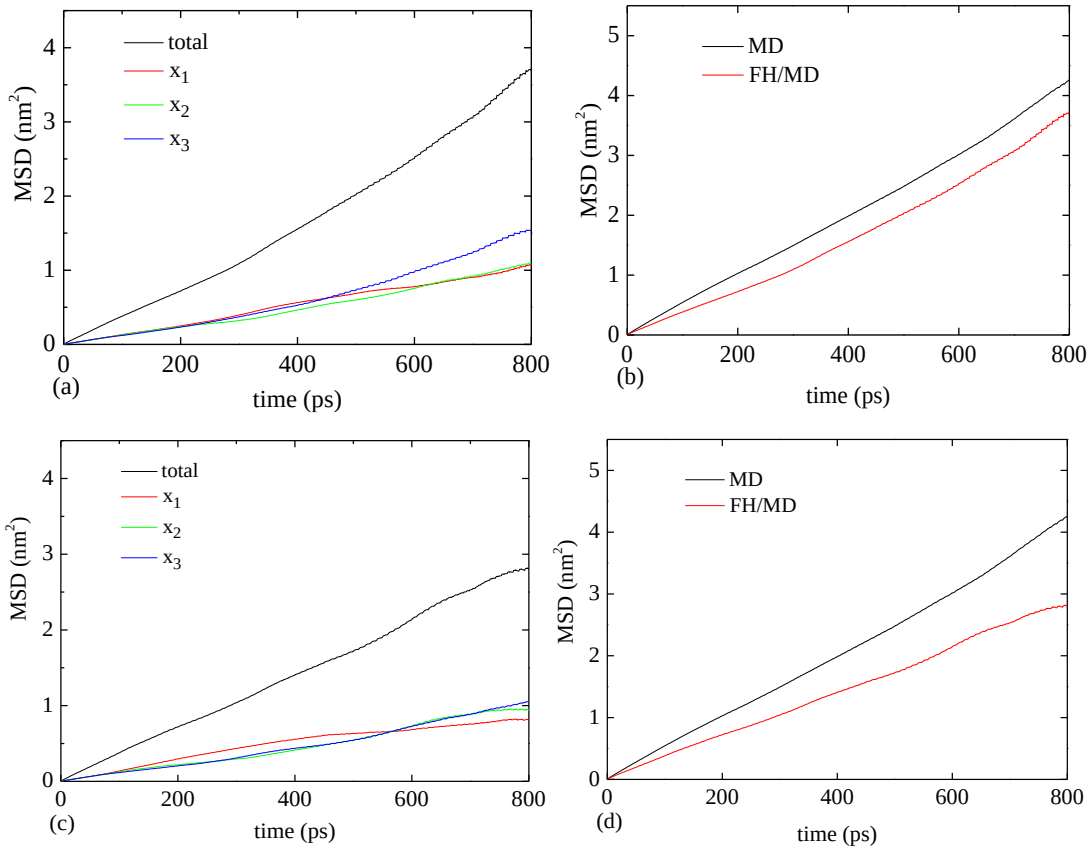

Fig.2 Isotropic molecular diffusion of one peptide in water: (a) the ensemble averaged mean square displacement (MSD) along the x_1, x_2 and x_3 directions and the total MSD of the hybrid FH/MD model, (b) comparison of the total MSD trajectories between the all-atom MD simulation and the FH/MD model at $\alpha = \beta = 40$ nm^2/ps. (c) and (d) are the same as (a) and (b) but at $\alpha = \beta = 60$ nm^2/ps

To simulate the diffusion of two peptide molecules in water (15b), a duplicate of the first peptide is introduced in the same computational box filled with water. In order to analyse the effect of the initial peptide location on its diffusion, two scenarios are simulated so that after the initial MD equilibration step: (i) one peptide (P1) is initialised near the domain centre, $\frac{2x_3}{L} = -0.175$, and the other (P2) is closer to the boundary, which would correspond to the edge of the flow, $\frac{2x_3}{L} = -0.875$, and (ii) both peptides are initialised close to the centre by keeping the peptide P1 location the same while adjusting the P2 location to $\frac{2x_3}{L} = 0.075$.

Following the discussion about the hybrid model sensitivity, in comparison with the one peptide -in-water system case (Fig.2b,d), the calibration parameters of the model for the two-

peptide system has been readjusted for best accuracy. While the size of the pure MD zone remains same, $R_{MD} = 0.5L/2$, the buffer MD/FH zone is reduced to $R_{FH} = 0.7L/2$ and the coupling constants are adjusted to $\alpha = \beta = 60$ nm^2/ps.

Fig.3 shows the resulting time dependency of the ensemble averaged MSD for three different directions and the total MSD from FH/MD model for the two peptides' system corresponding to initial conditions (i). Similar to the one peptide diffusion, the MSD trajectories do not show any significant anisotropy for either P1 or P2. In addition, the results for P1 and P2 are very similar as expected for the molecular diffusion in equilibrium conditions. The now-flow results for initial conditions (ii) are almost identical to the results for P1 (Fig.3a,b), hence, are not shown. Altogether this confirms that the hybrid FH/MD model parameters have been calibrated correctly.

Similar to the one peptide system, the diffusion coefficient is calculated from the slope of the MSD trajectory (Fig.6b,d) and compared with the results of the all-atom MD simulation. The diffusion coefficient obtained from the all-atom MD model are 0.89×10^{-5} and 0.65×10^{-5} cm^2/s for peptides P1 and P2. This should be compared with the diffusion coefficients of the FH/MD model, 1.05×10^{-5} and 0.82×10^{-5} cm^2/s, respectively, which are obtained for the same two peptides.

It can be noted that, since the two peptide molecules are identical and the diffusion is isotropic, any difference between the diffusion coefficients of the two peptides should be associated with the insufficient ensemble averaging due to the shortness of the MD simulation time. While the diffusion results of the one peptide system between the FH/MD model and the all-atom MD agree within 18%, for the two- peptide system, the discrepancy for P2 in comparison with the all-atom MD solution is increased to 25%. This is in agreement with [51] who suggested an additional correction for finiteness of the periodic box domain when computing molecular diffusion coefficients of complex fluids such as polymer chains in water.

Nevertheless, having considered the difference between the diffusion coefficients of the P1 and P2 peptides in the all-atom MD simulation, 0.14×10^{-5} cm^2/s as a measure of the statistical averaging error, the diffusion coefficients of the two peptide systems are in a reasonable agreement with the results of the single peptide diffusion. Hence, the suggested FH/MD model can be assumed to be validated for the considered case of the dilute solution of peptides in water.

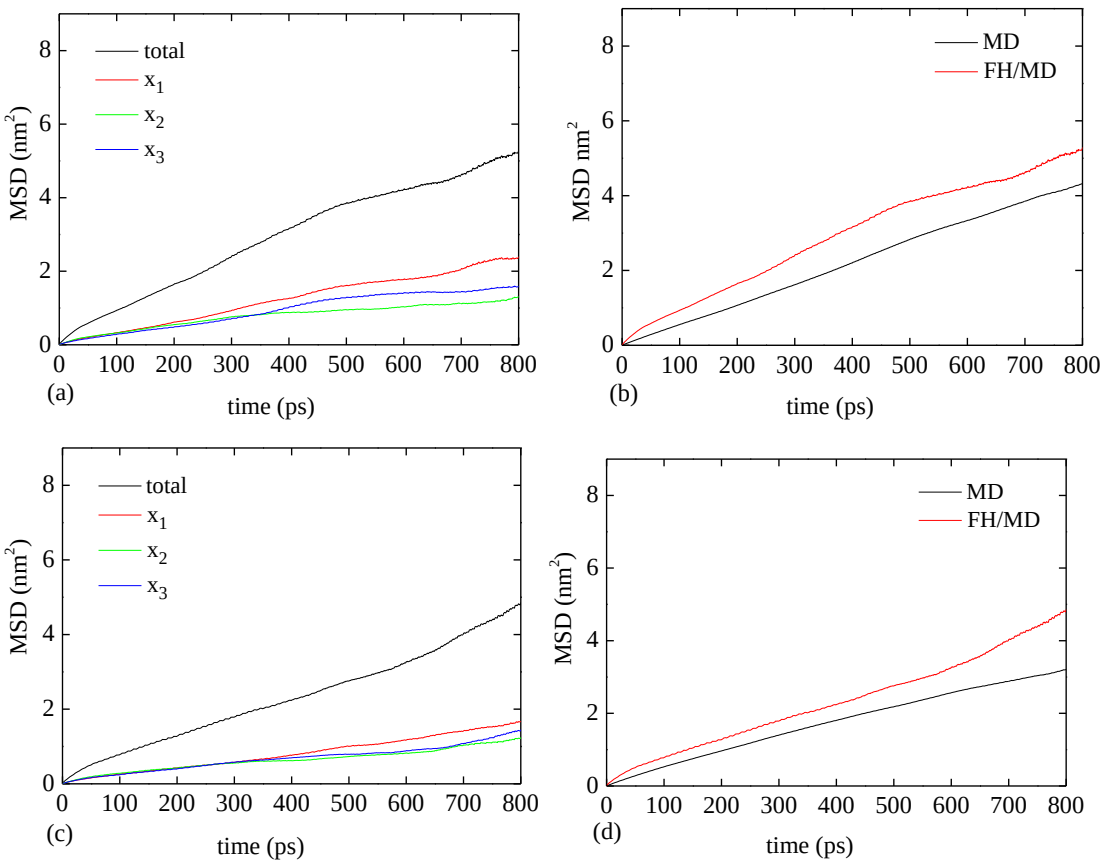

Fig.3 Isotropic molecular diffusion of two peptides in water corresponding to initial conditions (i): (a) and (c) are the ensemble averaged mean square displacement (MSD) along x_1, x_2 and x_3 direction and the total MSD from FH/MD model for peptide P1 and where (b),(d) stand for the same quantities for peptide P2. MSD trajectories obtained from the reference all-atom MD simulations are provided in each case.

3.2 Diffusion of one and two peptides in periodic Poiseuille flow

Having validated the hybrid FH/MD model for the one- and two- peptide systems without flow, the same systems are simulated in the Poiseuille flow in accordance with Eq(7) and for the pre-selected coupling parameters of the hybrid model based on the equilibrium simulations.

Six different flow regimes are considered corresponding to a range of Reynolds numbers corresponding to the maximum flow velocity, u_{max} = 0.03, 0.04, 0.055, 0.07, 0.075 and 0.1 nm/ps.

In order to ensure that the prescribed bulk flow regime is accurately implemented in each case, the simulation domain is broken down into several bins in the vertical direction, x_3, and the velocity profile of MD particles averaged in each bin and also the simulation time, u_1, is plotted

as a function of vertical coordinate. To collapse the data from the six different velocity regimes, all velocities are normalised by the corresponding u_{max} in each case. The resulting dimensionless velocity profiles for the one- and two- peptide systems are shown in Fig.4a and b. The results shown in Fig.4b correspond to the initial peptide conditions (i). Results of the two- peptide system simulation for the configuration (ii) are virtually the same. All solutions of the hybrid FH/MD model are in good agreement with the analytical Poiseuille flow profile.

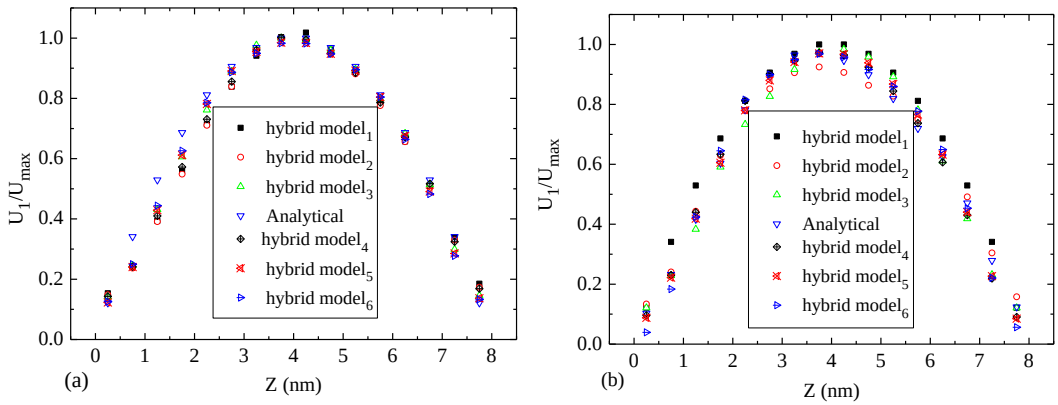

Fig.4 Comparison of the mean-flow velocity profile obtained by bin and time averaging of the MD particles of the hybrid FH/MD solution with the analytical model for the one- (a) and the two-peptide - system (b). All velocities have been normalised by the maximum velocity of the parabolic flow profile in each case: 0.03nm/ps (hybrid model$_1$), 0.04 (hybrid model$_2$), 0.055 (hybrid model$_3$), 0.07 (hybrid model$_4$), 0.075 (hybrid model$_5$) and 0.1 nm/ps (hybrid model$_6$).

As the next step, diffusion of one peptide in the Poiseuille flow is simulated for the same range of flow velocities. The averaged total MSD of the peptide and its x_1 coordinate are shown in Fig.5 (a) and (b) for flow velocities 0.055 and 0.1 nm/ps. Fig.5 (c) to (f) show the x_2 and x_3 components for the flow velocities 0.055, 0.07, 0.075, and 0.1 nm/ps. In comparison with Fig.2 (a), the MSD trajectory in Fig.5 (a) and (b) is of convective type (shows faster than linear growth) in the stream-wise direction, x_1. This can be attributed to the convection effect that reinforces the diffusion in this direction. Another observation from Fig.5 (c) to (f) is that the molecular diffusion in the shear gradient direction, x_3, i.e. the lateral migration, is faster in comparison with the diffusion of the homogeneous flow direction, x_2.

Interestingly, in comparison with the diffusion in the homogeneous direction, the lateral diffusion increases with the shear rate magnitude: the lateral migration accelerates near the valleys

of the Poiseuille flow, where the shear is strongest. The lateral migration seems to exhibit a change from the diffusive type (near the peak of the flow profile) to the convective type (near the valleys of the flow), which will be quantified in the future work, since the lateral migration has an important application in microfluidic devices [52].

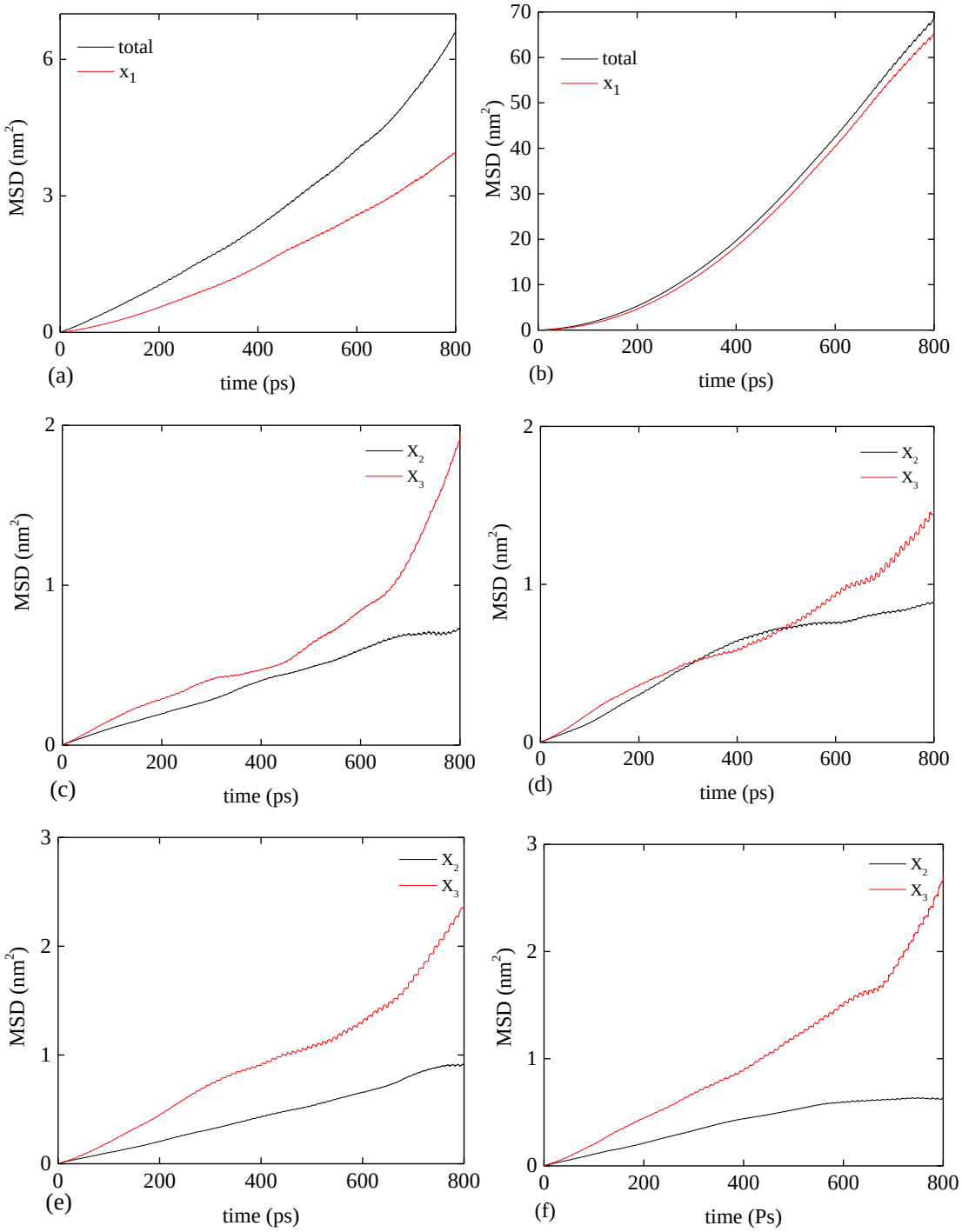

Fig.5 Diffusion of the single peptide in Poiseuille water flow: the ensemble averaged mean square displacement (MSD) in the x_1 and the total MSD trajectories for u_{max} = 0.055 (a), 0.1 nm/ps

(b). The MSD in the x_2 and x_3 directions are shown for u_{max} = 0.055 (c), 0.07(d), 0.075(e), and 0.1 nm/ps (f).

In order to analyse the molecular diffusion process in the flow, the root-mean-square of the convection speed, $\mathrm{r.m.s.}(u_{1c})$ is calculated from the MSD trajectories (Appendix A, Eq(A7)) for different flow velocities and plotted as a function of Reynolds number $R = \frac{u_{max}L}{\nu}$ in Fig.6a. $\mathrm{R.m.s.}(u_{1c})$ can be regarded as an effective convection speed of the peptide in the transversely non-uniform flow. It can be noted that the effective convection speed is approximately constant at Reynolds numbers lower than 0.5 and then rapidly increases as the Reynolds number exceeds 0.5. The increase of the effective convection speed indicates a prominent amplification of the molecular diffusion in the stream-wise direction due to the inertial flow effect.

To further analyse the lateral migration of the peptide molecule from the initial location to the equilibrium position in the x_3 direction, i.e. dimensionless distance of the lateral peptide migration, φ, is calculated from the MSD trajectory in the lateral direction (Appendix A, Eq(A8)). In accordance with the definition of the φ-function, for the initial location in the channel centre $x_3 = 0$, dimensionless distance $\varphi = 1$ corresponds to the edge of the flow where $x_3/L = \pm 0.5$.

Fig.6b shows as the Reynolds number increases, the peptide tends to migrate closer to the boundary, where the shear flow velocity gradient, $\frac{d}{dx_3}u_1 = -\frac{dp/dx_1}{\mu}x_3$ becomes negative in comparison with the zero value at $x_3 = 0$. This suggests that the lateral migration occurs in the direction against the shear gradient, which effect becomes stronger with the pressure gradient, dp/dx_1 thereby increasing with the Reynolds number.

It can also be noted that, for Reynolds numbers smaller than 0.5, the peptide tends to diffuse towards the flow boundary very slowly in comparison with the larger Reynolds number cases. It can be suggested that in the low Reynolds number case, the lateral migration is not flow related but rather attributed to the Brownian motion, which effect can also be investigated in future work.

In addition, it can be noted that in the experiment reported in [53] the particles initially uniformly distributed across the channel gradually migrate to the boundary of the channel with the increase of the Reynolds number from 0.36 to 14. Hence, despite having the same trend with regards to the Reynolds number, the lateral migration in the experiment [53] starts at the Reynolds

number much larger than the simulated Reynolds number in the present work. The discrepancy in the Reynolds number regime between the experiment and the simulation is attributed to the difference between the particle size: the peptides considered in the current work are much smaller in comparison with the particles used in [53]. This consideration is consistent with the experimental results [52], which showed that small particles tend to have faster lateral migrations in comparison with large particles at same Reynolds number. Furthermore, the increase of the lateral migration with the Reynolds number captured by the present multi-scale model is in good agreement with the continuum theory [54] as well as with the experiments on diffusion of micrometer-size [55] and nanometer–size [56] particles.

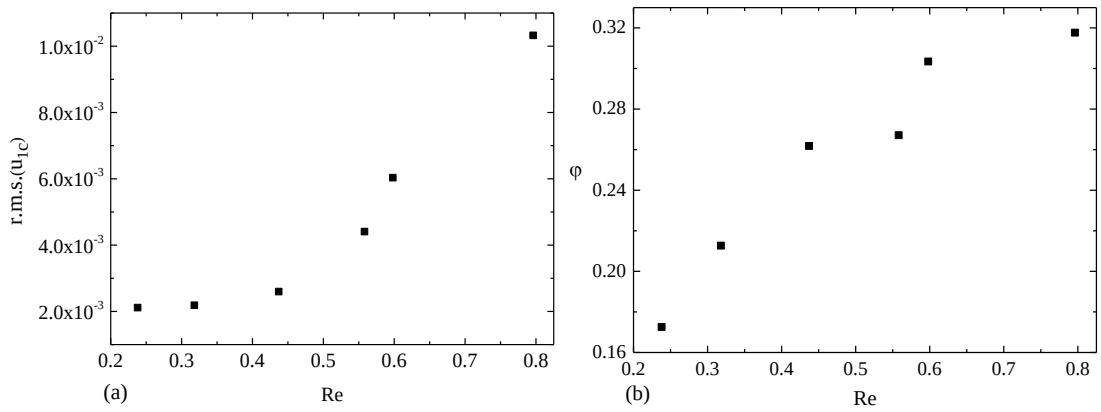

Fig.6 Effect of the Reynolds number on the stream-wise and lateral diffusion of one peptide in Poiseuille flow: (a) effective convection velocity of the peptide $\mathrm{r.m.s}(u_{1c})$ and (b) dimensionless distance of the lateral migration, φ.

Let's now discuss results for the two peptides in Poiseuille flow in case of the initial peptide conditions (i) where peptide molecule P1 is inserted in the centre of the channel while where the flow velocity is close to u_{max} and amino acid P2 is placed close to the boundary.

Fig.7 show the MSD trajectories in the three coordinate directions for P1 (panels (a-b)) and P2 (panels (c-d)) amino acids for three representative flow rates corresponding to u_{max} = 0.07, 0.075 and 0.1 nm/ps. Similar to the results for the one peptide system, the MSD in the stream-wise direction, x_1 shows a faster than linear growth for both P1 and P2 peptides. The growth is notably faster in comparison with the diffusion in the tangential flow directions. Again, this is attributed to the convection effect, where the fluid inertia enhances diffusion in the flow direction.

Similar to the one peptide system, for all flow rates, the MSD trajectory of peptide P1 shows

a faster diffusion in the lateral direction, x_3 in comparison with the homogeneous flow direction, x_2. In contrast to P1, the diffusion of peptide P2 in the shear gradient direction has a similar rate to the diffusion in the x_2 direction, which suggests the lateral diffusion speed depends on the initial location of the peptide.

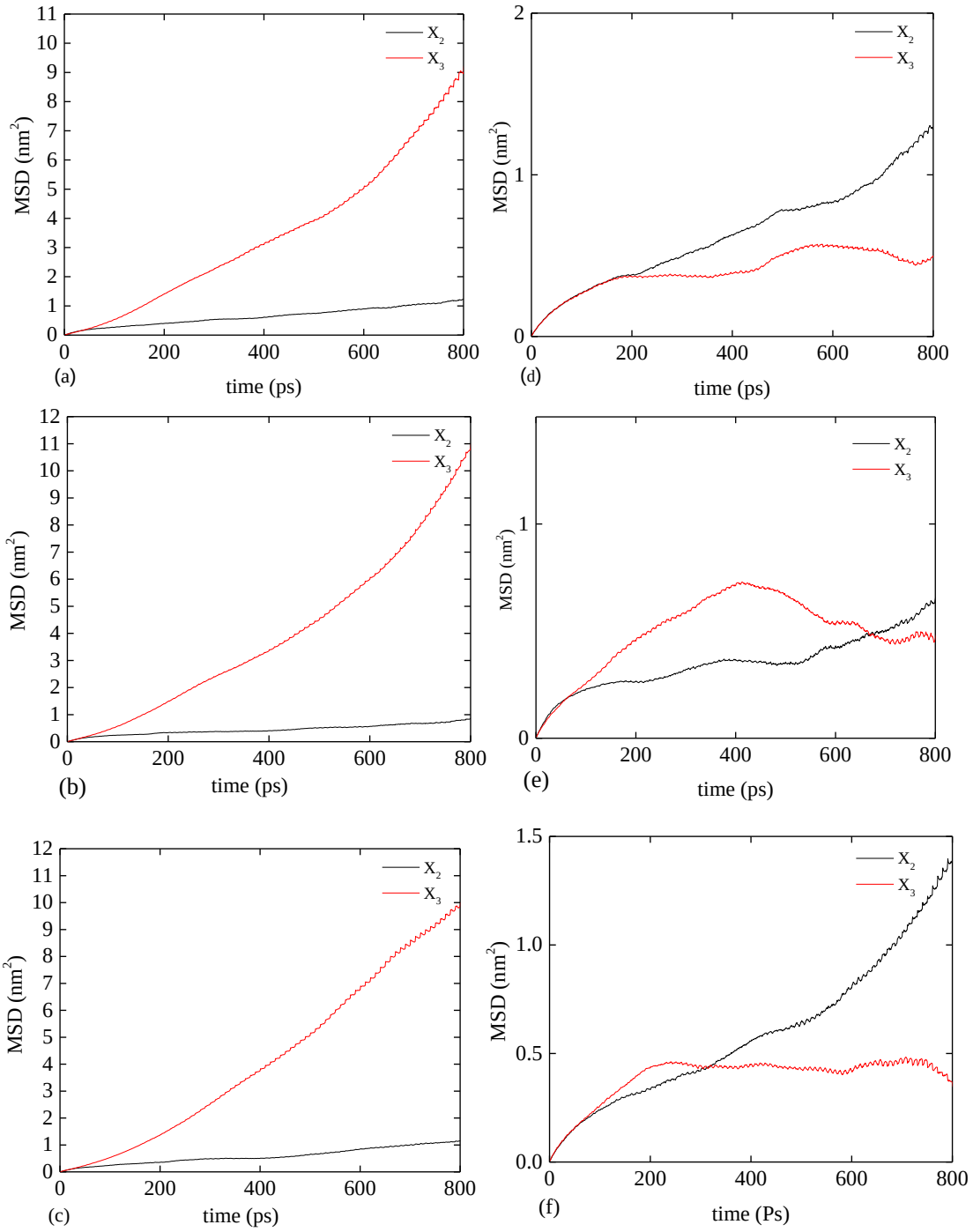

Fig.7 Diffusion of two peptides in water in Poiseuille flow corresponding to initial conditions (i): the ensemble averaged mean square displacement (MSD) in the x_2 and x_3 directions and the total MSD trajectories for a range of flow regimes, u_{max} = 0.07 (a) and (d), 0.075(b) and (e), and

0.1 nm/ps (c) and (f). (a,b,c) correspond to peptide P1 and (d,e,f) stands for peptide P2.

To further quantify the diffusion behavior of peptides P1 and P2, the effective convection speed, $\mathrm{r.m.s.}(u_{1c})$ and the dimensionless distance, φ are calculated for each case. Results for different Reynolds numbers are presented in Fig.8.

For both peptides, $\mathrm{r.m.s}(u_{1c})$ shows a similar approximately linear increase with the Reynolds number. This confirms that the inertia flow effect on the peptide diffusion in the stream-wise direction does not depend on the initial amino acid location, as expected since in this case the diffusion is normal to the shear gradient. In comparison with this, the lateral distance φ has a completely different behavior for the two peptide system. In the P1 case (Fig.9, small balls with bonds), which peptide mainly diffuses against the shear flow gradient direction, φ increases with the Reynolds number similar to the one- peptide system diffusion (comp. with Fig.6b). However, for the P2 case (Fig.9, large balls no bonds), φ takes a small value that virtually does not depend on the Reynolds number. In this case, peptide P2 was initially located close to the edge of the flow, where the shear flow gradient, $\frac{d}{dx_3}u_1$ reaches its negative peak value. In this case, any notable lateral migration of the peptide could only happen towards the channel centre, which would be in the direction of the shear gradient. However, such migration does not happen, and the 'large ball' peptide keeps jumping between the top and the bottom periodic boundary condition corresponding to the valleys of the periodic Poiseuille flow. This suggests that the lateral diffusion process of peptide molecules has a preferred direction always against the shear.

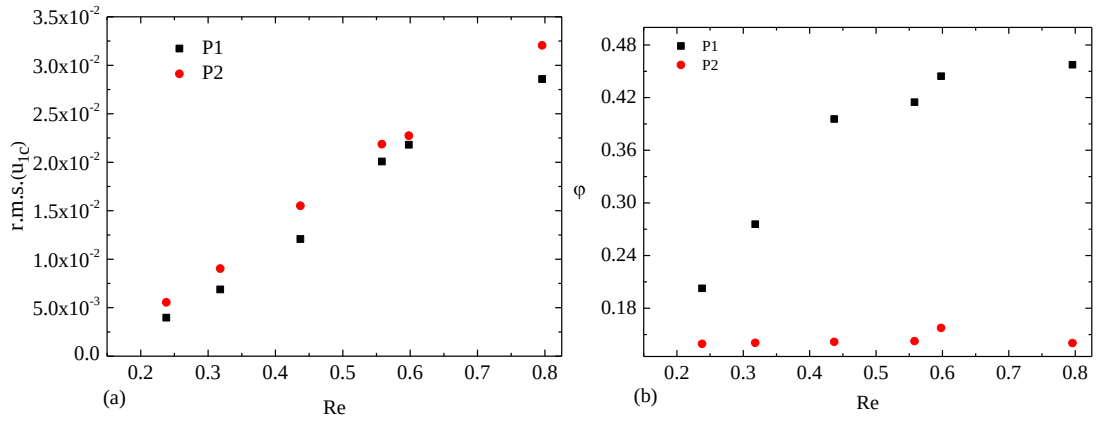

Fig.8 Effect of the Reynolds number on the stream-wise and lateral diffusion of two peptides in

Poiseuille flow corresponding to initial conditions (i): (a) effective convection velocity of the peptide $\mathrm{r.m.s}(u_{1c})$ and (b) dimensionless distance of the lateral peptide migration, φ.

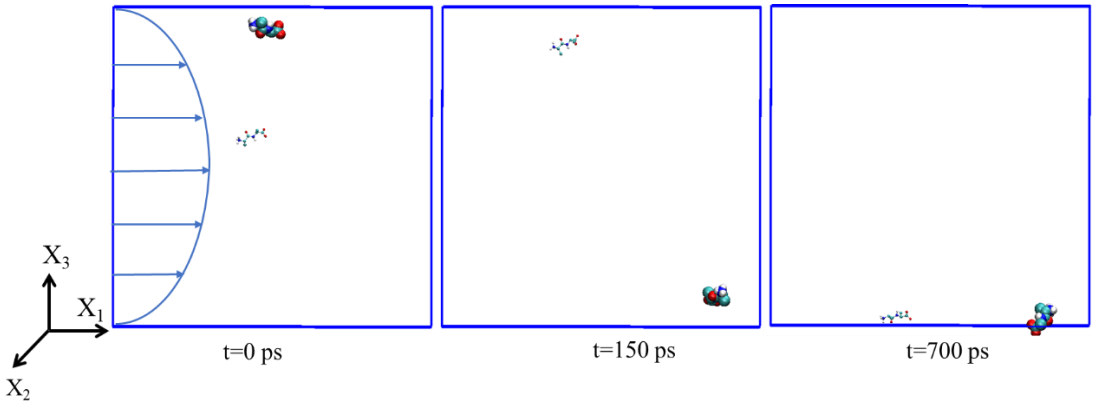

Fig.9 Evolution of two peptides starting from initial conditions (i) in Poiseuille flow at u_{max}= 0.1 nm/ps. Atoms of peptide P1 are shown by small balls and bonds and those of peptide P2 are depicted by large balls and no bonds. The flow velocity profile is shown in the left snapshot for reference.

To further confirm that the lateral migration of peptides is enhanced in the direction against the shear gradient, the diffusion of two peptides in the same Poiseuille flow is considered for initial conditions (ii). In this case both peptides are initially located near the centre of the channel.

The results are shown in Fig. 10, which should be compared with Fig.8 for the same peptide system at different initial conditions. It can be noted that when both the P1 and P2 peptides are initialised at a similar vertical coordinate in the flow velocity profile their diffusion properties are also very similar not only in the stream-wise direction but also in the shear-gradient direction. For both the peptides, the diffusion rate increases with the flow Reynolds number and the functional dependencies of $\mathrm{r.m.s}(u_{1c})$ and φ of each peptide are similar to those of one diffusing peptide (comp. with Fig.6). The revealed similarity with the one- peptide system suggests that peptide-peptide interaction has a negligible effect for the considered two-peptide system in comparison with the lateral migration due to the shear effect.

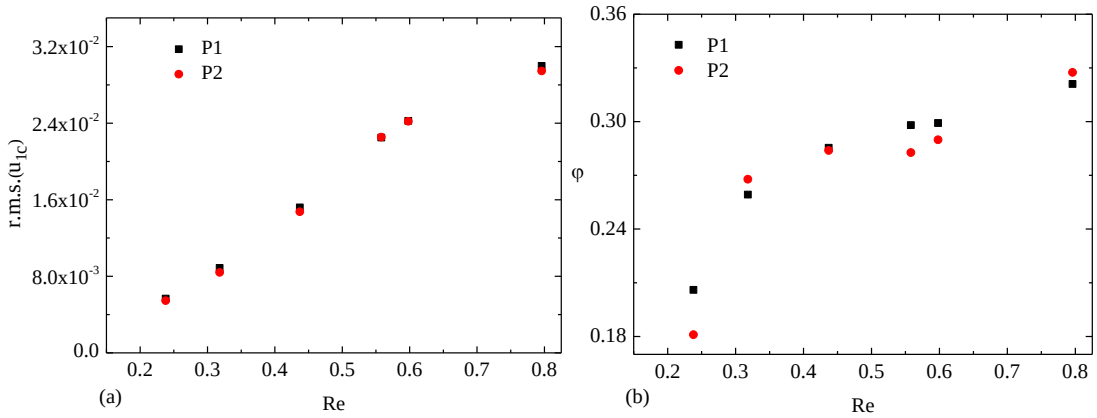

Fig.10 Effect of the Reynolds number on the stream-wise and lateral diffusion of two peptides in Poiseuille flow corresponding to initial conditions (ii): (a) effective convection velocity of the peptide $\mathrm{r.m.s}(u_{1c})$ and (b) dimensionless distance of the lateral migration, φ.

3.3 Comparison of computational costs between MD and FH/MD for one peptide diffusing in Poiseuille flow

One of the advantages of the FH/MD method in comparison with the single-scale atomistic-resolution methods such as Non-Equilibrium Molecular Dynamics (NEMD) is the greatly reduced computational cost. For example, in [57] the authors performed a NEMD of the Couette flow of water atoms in a microscopic channel between two sliding graphene walls at room temperature conditions. Due to the statistical noise associated with the thermal atom fluctuations, the statistical convergence of the NEMD solution for a non-uniform flow profile was shown to be limited to relatively large flow speeds, e.g. $U_{flow} \geq 50\ m/s$. This is because, when computing the time-averaged flow velocity $U_{flow} = U_{flow}(x_3)$, the thermal-noise induced velocity fluctuation, δU_{flow} scales as

$$\delta U_{flow} = \frac{A \cdot U_{thermal}}{\sqrt{N_{NEMD} \cdot M_{bin}}} \tag{17}$$

where N_{NEMD} is the number of MD time steps, M_{bin} is the number of MD atoms per the sampling bin volume, $U_{thermal}$ is the characteristic thermal velocity of water atoms (which from the equipartition theorem can be estimated to be $585\ m/s$), and A is a proportionality parameter depending on the chemical potentials of the simulated water system.

In the NEMD simulations of Couette water flow [57], the solution averaging over 10^6 MD steps was required to converge the error down to 10% of $U_{flow} = 50\ m/s$. The averaging bin size considered in [57] is approximately the same as in the current work. Furthermore, assuming the

same parameter A holds for NEMD simulations of water atoms at the same room temperature conditions, Eq(17) can be inverted to calculate the number of NEMD time steps required for the statistical convergence within 10% of the peak velocity of the Poiseuille flow, $U_{flow} = \max(\boldsymbol{u}^{Poiseuille})$,

$$N_{NEMD} = {M_{bin}}^{-1}\left(\frac{A \cdot U_{thermal}}{0.1 \cdot U_{flow}}\right)^2. \quad (18)$$

The results of applying Eq(18) to the Poiseuille flows considered in Section 3.2 are summarised in Table 1. The table takes into account that the computational cost of the FH/MD method is mostly dominated by the MD part of the solution, and the cost of solving the modified MD equations (5),(6) per time step is about 19% higher in comparison with that of the pure MD solution for the same number of atoms. All run times correspond to the simulations performed on 32 CPU cores in GROMACS. Notably, in comparison with the all-atom NEMD method, the cost of the multiscale solution does not scale with the flow velocity. Depending on the flow regime, the computational cost of the all-atom NEMD simulations for the same molecular system corresponds to a 2- to 20-fold increase in comparison with the multiscale solution (FH/MD).

Table 1. Evaluation of the computational efficiency of the FH/MD method in comparison with the all-atom NEMD method for the single peptide diffusion in Poiseuille flow.

Peak flow velocity (m/s)	NEMD steps required, x10^6	MD computational run times, hours	FH/MD steps, x10^6	FH/MD computational run times, hours
30	27	7.5	1	0.32
40	15	4.2	1	0.32
55	8.2	2.2	1	0.32
75	4.4	1.2	1	0.32
100	2.5	0.67	1	0.32

Conclusion

A hybrid multiscale model is implemented to simulate the diffusion process of one and two

peptide molecules in Poiseuille flow. Characteristic feature of the new model includes the resolution of inter-atomic forces between the migrating biomolecules and the surrounding water atoms with consistently accounting for the non-uniform bulk flow at several Reynolds numbers. The model represents an extension of the previously developed hybrid multiscale method based on coupling Molecular Dynamics (MD) and Fluctuating Hydrodynamics (FH) simulations of the same complex fluid [41, 45] to multiple moving peptide molecules solvated in water and subjected to Poiseuille flow. The hybrid model has been validated in comparison with the all-atom MD simulation for the no flow case and in comparison with the analytical Poiseuille flow velocity profile.

The effect of the flow Reynolds number of peptide diffusion in Poiseuille flow has been investigated. First, it is shown that, irrespective of the initial peptide location in the channel, the inertial flow effect always leads to a faster than linear growth of the Mean Square Deviation (MSD) trajectory in the stream-wise direction. Secondly, the lateral peptide migration strongly depends on the shear flow velocity gradient: while the lateral diffusion against the shear gradient is enhanced as the Reynolds number increases, the lateral diffusion in the direction of the shear gradient is suppressed regardless of the Reynolds number. This leads to a sensitivity of the lateral migration of peptides to the initial location where the biomolecules are injected in the non-uniform flow profile.

The computational efficiency of the suggested FH/MD method is compared with the all-atom Non-Equilibrium MD (NEMD) based on the thermal velocity scaling, where the scaling parameter is evaluated from the previous NEMD simulation of a uniform shear water flow. It is shown that the computational cost of the all-atom NEMD simulations for the current system is expected to be a factor of 2 to 20 greater in comparison with the suggested FH/MD method. Notably, in contrast to the all-atom NEMD methods, the cost of the multiscale solution does not scale with the flow velocity.

Remarkably, the sensitivity of lateral diffusion transport of small peptides to the shear flow gradient in Poiseuille flow was previously predicted using a continuum diffusion theory based on the rigid sphere model [54,58]. The current atomistic-scale resolving simulation results confirm the same effect at the nanoscale level, where assumptions of the continuum theory break down. Further work will be devoted to a detailed study of the peptide structure such as the Ramachandran plot of the peptide angles under the non-uniform flow effect. For example, the

effect of the shear on the peptide structure can be expected to have important implications for protein delivery in medical devices.

Acknowledgement

The work of F.L. was supported by the China Scholarship Council (CSC). I.A.K. and S.A.K. gratefully acknowledge the funding under the European Commission Marie Skłodowska-Curie Individual Fellowship Grant No. H2020-MSCA-IF-2015-700276 (HIPPOGRIFFE). V. F. thanks Ministry of Education and Science of Ukraine for financial support in the frame of project "Novel nanomaterials based on the lyophilic self-assembled systems: theoretical prediction, experimental investigation and biomedical applications" (0120U101064). The work was also supported by European Commission in the framework of the RISE program, Grant No. H2020-MSCA-RISE-2018-824022-ATM2BT and utilised Queen Mary's Apocrita HPC facility, supported by QMUL Research-IT [59].

The authors are greatful to Dr Dmitry Nerkuh from Aston University, UK for helpful comments and discussion.

Data Availability

The data that support the findings of this study are available from the corresponding author upon reasonable request

References

1. Sanders, G.H.W. and A. Manz, *Chip-based microsystems for genomic and proteomic analysis.* TrAC Trends in Analytical Chemistry, 2000. **19**(6): p. 364-378.
2. DeWitt, S.H., *Microreactors for chemical synthesis.* Current opinion in chemical biology, 1999. **3**(3): p. 350-356.
3. Mach, A.J. and D. Di Carlo, *Continuous scalable blood filtration device using inertial microfluidics.* Biotechnology and Bioengineering, 2010. **107**(2): p. 302-311.
4. Gossett, D.R., et al., *Inertial Manipulation and Transfer of Microparticles Across Laminar Fluid Streams.* Small, 2012. **8**(17): p. 2757-2764.
5. Segre, G. and A. Silberberg, *Behaviour of macroscopic rigid spheres in Poiseuille flow. Part 1. Determination of local concentration by statistical analysis of particle passages through crossed light beams.* Journal of Fluid Mechanics, 1962. **14**: p. 115.
6. Phillips, R.J., et al., *A constitutive equation for concentrated suspensions that accounts for shear-induced particle migration.* Physics of Fluids A: Fluid Dynamics, 1992. **4**(1): p. 30-40.

7. Nott, P.R. and J.F. Brady, *Pressure-driven flow of suspensions: simulation and theory.* Journal of Fluid Mechanics, 1994. **275**: p. 157-199.

8. Morris, J.F. and F. Boulay, *Curvilinear flows of noncolloidal suspensions: The role of normal stresses.* Journal of Rheology, 1999. **43**(5): p. 1213-1237.

9. Shapley, N.C., R.A. Brown, and R.C. Armstrong, *Evaluation of particle migration models based on laser Doppler velocimetry measurements in concentrated suspensions.* Journal of Rheology, 2004. **48**(2): p. 255-279.

10. Miller, R.M. and J.F. Morris, *Normal stress-driven migration and axial development in pressure-driven flow of concentrated suspensions.* Journal of Non-Newtonian Fluid Mechanics, 2006. **135**(2): p. 149-165.

11. Miller, R.M., J.P. Singh, and J.F. Morris, *Suspension flow modeling for general geometries.* Chemical Engineering Science, 2009. **64**(22): p. 4597-4610.

12. Mirbod, P., *Two-dimensional computational fluid dynamical investigation of particle migration in rotating eccentric cylinders using suspension balance model.* International Journal of Multiphase Flow, 2016. **80**: p. 79-88.

13. Ingber, M.S., et al., *An improved constitutive model for concentrated suspensions accounting for shear-induced particle migration rate dependence on particle radius.* International Journal of Multiphase Flow, 2009. **35**(3): p. 270-276.

14. Baghban, A., et al., *Estimation of oil and gas properties in petroleum production and processing operations using rigorous model.* Petroleum Science and Technology, 2016. **34**(13): p. 1129-1136.

15. Aminfar, H. and R. Motallebzadeh, *Numerical Investigation of the Effects of Nanoparticle Diameter on Velocity Field and Nanoparticle Distribution of Nanofluid Using Lagrangian-Eulerian Approach.* Journal of Dispersion Science and Technology, 2011. **32**(9): p. 1311-1317.

16. Singh, P.K., et al., *Experimental and Numerical Investigation Into the Heat Transfer Study of Nanofluids in Microchannel.* Journal of Heat Transfer, 2011. **133**(12).

17. Lin, Y.-C. and C.-P. Jen, *Mechanism of hydrodynamic separation of biological objects in microchannel devices.* Lab on a Chip, 2002. **2**(3): p. 164-169.

18. Kim, M.-m. and A.L. Zydney, *Theoretical analysis of particle trajectories and sieving in a two-dimensional cross-flow filtration system.* Journal of Membrane Science, 2006. **281**(1): p. 666-675.

19. Ahlrichs, P. and B. Dünweg, *Simulation of a single polymer chain in solution by combining lattice Boltzmann and molecular dynamics.* The Journal of Chemical Physics, 1999. **111**(17): p. 8225-8239.

20. Lyulin, A.V., D.B. Adolf, and G.R. Davies, *Brownian dynamics simulations of linear polymers under shear flow.* The Journal of Chemical Physics, 1999. **111**(2): p. 758-771.

21. Cui, W., et al., *Effect of chaotic movements of nanoparticles for nanofluid heat transfer augmentation by molecular dynamics simulation.* Applied Thermal Engineering, 2015. **76**: p. 261-271.

22. Hu, C., et al., *Molecular dynamics simulation on the friction properties of nanofluids confined by idealized surfaces.* Tribology International, 2014. **78**: p. 152-159.

23. Ren, W. and W. E, *Heterogeneous multiscale method for the modeling of complex fluids and micro-fluidics.* Journal of Computational Physics, 2005. **204**(1): p. 1-26.

24. Yasuda, S. and R. Yamamoto, *A model for hybrid simulations of molecular dynamics and computational fluid dynamics.* Physics of Fluids, 2008. **20**(11): p. 113101.

25. Borg, M.K., D.A. Lockerby, and J.M. Reese, *A multiscale method for micro/nano flows of high aspect ratio.* Journal of Computational Physics, 2013. **233**: p. 400-413.

26. Borg, M.K., et al., *Multiscale simulation of water flow through laboratory-scale nanotube membranes.* Journal of Membrane Science, 2018. **567**: p. 115-126.

27. O'Connell, S.T. and P.A. Thompson, *Molecular dynamics--continuum hybrid computations: A tool for studying complex fluid flows.* Physical Review E, 1995. **52**(6): p. R5792-R5795.

28. Lifshitz, L.D.L.a.E.M., *Statistical Physics*. 1980, Amsterdam: Elsevier.

29. De Fabritiis, G., R. Delgado-Buscalioni, and P.V. Coveney, *Multiscale Modeling of Liquids with Molecular Specificity.* Physical Review Letters, 2006. **97**(13): p. 134501.

30. De Fabritiis, G., et al., *Fluctuating hydrodynamic modeling of fluids at the nanoscale.* Physical Review E, 2007. **75**(2): p. 026307.

31. Voulgarakis, N.K. and J.-W. Chu, *Bridging fluctuating hydrodynamics and molecular dynamics simulations of fluids.* The Journal of Chemical Physics, 2009. **130**(13): p. 134111.

32. FlekkØy, E.G., G. Wagner, and J. Feder, *Hybrid model for combined particle and continuum dynamics.* Europhysics Letters, 2000. **52**(3): p. 271-276.

33. Delgado-Buscalioni, R. and P.V. Coveney, *Continuum-particle hybrid coupling for mass, momentum, and energy transfers in unsteady fluid flow.* Physical Review E, 2003. **67**(4): p. 046704.

34. Nie, X.B., et al., *A continuum and molecular dynamics hybrid method for micro- and nano-fluid flow.* Journal of Fluid Mechanics, 2004. **500**: p. 55-64.

35. Praprotnik, M., L.D. Site, and K. Kremer, *Adaptive resolution molecular-dynamics simulation: Changing the degrees of freedom on the fly.* The Journal of Chemical Physics, 2005. **123**(22): p. 224106.

36. Delgado-Buscalioni, R., K. Kremer, and M. Praprotnik, *Concurrent triple-scale simulation of molecular liquids.* The Journal of Chemical Physics, 2008. **128**(11): p. 114110.

37. Pavlov, E., et al., *Visualising and controlling the flow in biomolecular systems at and between multiple scales: from atoms to hydrodynamics at different locations in time and space.* Faraday Discussions, 2014. **169**(0): p. 285-302.

38. Scukins, A., et al., *Multiscale molecular dynamics/hydrodynamics implementation of two dimensional "Mercedes Benz" water model.* The European Physical Journal Special Topics, 2015. **224**(12): p. 2217-2238.

39. Korotkin, I.A. and S.A. Karabasov, *A generalised Landau-Lifshitz fluctuating hydrodynamics model for concurrent simulations of liquids at atomistic and continuum resolution.* The Journal of Chemical Physics, 2018. **149**(24): p. 244101.

40. Markesteijn, A., et al., *Concurrent multiscale modelling of atomistic and hydrodynamic processes in liquids.* Philosophical Transactions of the Royal Society A: Mathematical, Physical and Engineering Sciences, 2014. **372**(2021).

41. Korotkin, I., et al., *A hybrid molecular dynamics/fluctuating hydrodynamics method for modelling liquids at multiple scales in space and time.* The Journal of Chemical Physics, 2015. **143**(1): p. 014110.

42. Korotkin, I., et al., *Two-phase flow analogy as an effective boundary condition for modelling liquids at atomistic resolution.* Journal of Computational Science, 2016. **17, Part 2**: p. 446-456.

43. Tarasova, E., et al., *Complete virus capsid at all-atom resolution: Simulations using molecular dynamics and hybrid molecular dynamics/hydrodynamics methods reveal semipermeable membrane function.* Journal of Molecular Liquids, 2017. **245**: p. 109-114.

44. Van Der Spoel, D., et al., *GROMACS: Fast, flexible, and free.* Journal of Computational Chemistry, 2005. **26**(16): p. 1701-1718.

45. Hu, J., I.A. Korotkin, and S.A. Karabasov, *Hybrid multiscale simulation reveals focusing of a diffusing peptide molecule by parallel shear flow in water.* Journal of Molecular Liquids, 2019. **280**: p. 285-297.

46. F. Li , I.K., M. Taiji, S.Karabasov,, *A multi-scale and multi-physics Atomic Force Microscopy model for force calculations at atomistic resolution and realistic flow conditions, F. Li , I. Korotkin , M. Taiji, S.Karabasov.* under review.

47. *Hagen–Poiseuille equation (and laminar flow)*, in *Essential Equations for Anaesthesia: Key Clinical Concepts for the FRCA and EDA*, E.T. Gilbert-Kawai and M.D. Wittenberg, Editors. 2014, Cambridge University Press: Cambridge. p. 19-20.

48. Markesteijn, A.P., et al., *A new non-linear two-time-level Central Leapfrog scheme in staggered conservation–flux variables for fluctuating hydrodynamics equations with GPU implementation.* Computer Methods in Applied Mechanics and Engineering, 2014. **281**: p. 29-53.

49. Huang, W., Z. Lin, and W.F. van Gunsteren, *Validation of the GROMOS 54A7 Force Field with Respect to β-Peptide Folding.* Journal of Chemical Theory and Computation, 2011. **7**(5): p. 1237-1243.

50. Einstein, A., *On the Motion of Small Particles Suspended in Liquids at RestRequired by the Molecular-Kinetic Theory of Heat.* Annalen der Physik, 1905. **322**: p. 549-560.

51. Dünweg, B. and K. Kremer, *Molecular dynamics simulation of a polymer chain in solution.* The Journal of Chemical Physics, 1993. **99**(9): p. 6983-6997.

52. Kang, K., et al., *DNA-based highly tunable particle focuser.* Nature Communications, 2013. **4**(1): p. 2567.

53. Kim, Y.W., et al., *Inertial-microfluidic radial migration in solid/liquid two-phase flow through a microcapillary: Particle equilibrium position.* Experiments in Fluids, 2011. **51**(3): p. 723-730.

54. Schonberg, J.A. and E.J. Hinch, *Inertial migration of a sphere in Poiseuille flow.* Journal of Fluid Mechanics, 1989. **203**: p. 517-524.

55. Kim, Y.W. and J.Y. Yoo, *Transport of solid particles in microfluidic channels.* Optics and Lasers in Engineering, 2012. **50**(1): p. 87-98.

56. Liot, O., et al., *Transport of nano-objects in narrow channels: influence of Brownian diffusion, confinement and particle nature.* Journal of Physics: Condensed Matter, 2018. **30**(23): p. 234001.

57. Li, F., I.A. Korotkin, and S.A. Karabasov, *Rheology of Water Flows Confined between Multilayer Graphene Walls.* Langmuir, 2020. **36**(20): p. 5633-5646.

58. Hood, K., S. Lee, and M. Roper, *Inertial migration of a rigid sphere in*

three-dimensional Poiseuille flow. Journal of Fluid Mechanics, 2015. **765**: p. 452-479.

59. T. King, S.B., and L. Zalewski, *Apocrita—High Performance Computing Cluster for Queen Mary* University of London, 2017.

60. Elrick, D., *Source Functions for Diffusion in Uniform Shear Flow.* Australian Journal of Physics, 1962. **15**(3): p. 283-288.

61. Hess, S. and J.C. Rainwater, *Diffusion in a laminar flow: Shear rate dependence of correlation functions and of effective transport coefficients.* The Journal of Chemical Physics, 1984. **80**(3): p. 1295-1303.

Appendix A: Analytical model of molecular diffusion with including the flow effect

Following [45], the velocity of a diffusing particle is decomposed into the small-scale random diffusion velocity u_d, and the large-scale convection velocity component u_c, due to the bulk flow effect

$$\mathbf{u}_p = \mathbf{u}_d + \mathbf{u}_c, \tag{A1}$$

where $\mathbf{u}_c = (u_{1c}, 0,0)$ for the flow in the x_1 direction and $u_{1c} = u_{1c}(\boldsymbol{x}_p(t))$ since the particle convection speed induced by the flow depends on the particle coordinates in the flow.

As the next step, ensemble averaging over different realisations corresponding to different initial coordinates of water atoms in the MD simulation domain after the equilibration step, $< >$ is introduced. Due to the random character of the diffusion process, $< u_d >=0$, which leads to $<\mathbf{u}_p>= <\mathbf{u}_c>$.

The particle coordinate along flow direction is obtained by integrating Eq. (A1) in time

$$x_{1p}(t) = x_{1p}(0) + \int_0^t u_{1d} \cdot dt' + \int_0^t u_{1c} \cdot dt' \tag{A2}$$

which leads to

$$\langle \Delta x_1^2(t) \rangle = \left\langle \left(x_{1p}(t) - x_{1p}(0) \right)^2 \right\rangle \tag{A3}$$

and which can be further rearranged to

$$\langle \Delta x_1^2(t) \rangle = \left\langle \left(\int_0^t u_{1d} \cdot dt' + \int_0^t u_{1c} \cdot dt' \right)^2 \right\rangle. \tag{A4}$$

Considering that the random diffusion velocity has zero mean, $< u_{1d} >= 0$, and by rearranging right-hand side of Eq. (A4), an expression for the Mean Square Displacement (MSD) in the flow direction is obtained,

$$\langle \Delta x_1^2(t) \rangle = \left\langle \left(\int_0^t u_{1d} \cdot dt' \right)^2 \right\rangle + \left\langle \left(\int_0^t u_{1c} \cdot dt' \right)^2 \right\rangle, \tag{A5}$$

where $\langle (\int_0^t u_{1d} \cdot dt')^2 \rangle = \langle \Delta x_2^2(t) \rangle$ since the flow is homogenous in the x_2-direction, and $\langle (\int_0^t u_{1c} \cdot dt')^2 \rangle = \overline{u_{1c}^2} t^2$, wherein the overbar denotes ensemble averaging along the peptide trajectory. This leads to

$$\langle \Delta x_1^2(t) \rangle - \langle \Delta x_2^2(t) \rangle = \overline{u_{1c}^2} t^2. \tag{A6}$$

The above equation is identical to the one obtained from the continuum diffusion theory [60, 61]. And by introducing the root-mean-square value of the convection velocity, $\mathrm{r.m.s.}(u_{1c}) = \sqrt{\overline{u_{1c}^2}}$, (A6) is further rearranged to

$$\mathrm{r.m.s.}(u_{1c}) = \sqrt{\frac{\langle \Delta x_1^2(t) \rangle - \langle \Delta x_2^2(t) \rangle}{t^2}}. \tag{A7}$$

Eq. (A7) establishes a relationship between the MSD trajectories in the stream-wise and the homogeneous flow direction, x_1 and x_2, and the effective particle convection velocity, $\mathrm{r.m.s.}(u_{1c})$.

For diffusion in the lateral direction, x_3, the particle migration process can be further characterised by the dimensionless diffusion distance φ:

$$\varphi = \sqrt{\frac{\int_0^t \langle \Delta x_3^2(t) \rangle dt'}{\left(\frac{L}{2}\right)^2 \cdot t}} \tag{A8}$$

where L and t are the height of the flow channel in the x_3 direction and the simulation time, respectively.